5th International Conference
on
Wind Turbine Noise
Denver 28-30 August 2013

Broadband Noise Prediction of Small Horizontal Wind Turbine Rotor

Bavuudorj Ovgor Energy Engineering Program, Inha University, Incheon, 402-751, Republic of Korea

E-mail: bavuudorj@gmail.com

Seungbae Lee Department of Mechanical Engineering, Inha University, Incheon, 402-751, Republic of Korea

E-mail: sbaelee@inha.ac.kr

Summary

As small wind turbines are located much close to the residents, the emission level of such wind turbines becomes one of the major social issues. This paper presents the results of numerical prediction of small wind turbine rotor noise by using a Computational Fluid Dynamics (CFD) code and an in-house code for aero-acoustic calculation based on Ffowcs Williams-Hawking's (FW-H) equations. The wind turbine model has a three-bladed rotor of 1.5 m diameter. The flow-field around wind turbine rotor model was simulated by solving three-dimensional, unsteady, finite-volume formulated Reynolds-averaged Navier-Stokes equation with shear stress transport turbulence model, whereas far-field aero-acoustic analysis was performed by solving FW-H equations. The capabilities of in-house FW-H equation based code were validated acoustic signatures from vehicle engine cooling fan, which were measured by reverberant room method. The noise characteristics of three sets of blades with different twist and chord length distributions at a series of cross sections have been simulated and discussed.

1. Introduction

The numerical prediction of flow field and noise characteristics of wind turbines are complicated due to three-dimensional unsteady nature of flow formed around turbine blades. The literature review suggests that there are two different strategies prevalent in the numerical prediction of noise from wind turbine rotor (Casper Farassat 2002, Ianniello 2007, Lyrintintzis 1994). The first strategy is based on direct computation of aero-acoustic propagation by computational fluid dynamics code. The second strategy based on a hybrid approach which uses computational fluid dynamics solver for dynamic near-field flow simulation and separate Computational

Aero-Acoustic (CAA) solver for aero-acoustic simulation of sound propagation to the far field. The latter strategy is referred as hybrid CAA methods, and first strategy as direct CAA method in the literature. Although the direct CAA method is more accurate, it requires much more computational resources than the hybrid method. The main reasons for high computational cost are the unsteady nature of aero-acoustic phenomenon, large acoustic radiation field needed to be included to the simulation, and small acoustic energy in comparison with aerodynamic energy in the near-field. On the other hand the hybrid strategy requires high-resolution simulation only in dynamic near-field region and the far-field propagation is predicted by computationally cheap acoustic propagation equation. The hybrid aero-acoustic strategy using separate solvers for the simulation of dynamic field and acoustic propagation could be divided into two main methods: integral methods (acoustic analogies, Kirchhoff integral, Ffowcs William Hawking's equations) and Linearized Euler Equation (LEE) method (Bogey Bailly Juve 2002, Tadamasa Zangeneh 2011, Mo Lee 2011).

The aim of this paper is to report the comprehensive study on the noise prediction of small horizontal-axis wind turbine rotor by numerically solving near-field flow by incompressible finite-volume Navier-Stokes CFD solver and acoustic far-field propagation by numerical code based on FW-H equation solver. The actual noise characteristics of three different models of the small horizontal axis wind turbine rotor with the diameter of 1.5 m. The simulated noise characteristics of one blade model are compared with the experimentally observed noise data for the validation of the code.

2. Wind turbine rotor

The 500W small horizontal-axis wind turbine consists of 3 bladed rotor with 1.5 m diameter, 500W permanent magnet generator, and yawing system and tower. The actual turbine was built and tested experimentally at the Inha University. The wind turbine blade chord and twist angle distribution are shown in Fig.1 and Fig.2. The wind turbine blade profile is based on airfoil FX-63-137 from root to tip. The airfoil has 13.7% thickness of chord length and maximum thickness located at 29.7% of chord length.

To identify the performance and to validate CFD calculations the wind turbine has been tested in an open wind tunnel affiliated at the Inha University. The wind tunnel is a low speed tunnel with a cross section of 2.1 m by 2.3 m and permits continuous operation of wind speed from 0 to 16.7 m/s at a low level of turbulence intensity. The wind speed in the wind tunnel is automatically monitored by using a digital micro-manometer with a correction for density through the measurement of the room temperature and humidity. The 1.5 m diametered wind turbine can be placed as full scale inside the test section of the wind tunnel. The general schematic of the wind tunnel is shown in Fig.3.

In the scope of the current paper two types of experimental test have been conducted for performance evaluation of the wind turbine. At the first step, the rotor performance was evaluated by use of torque meter and power braking system, and at the second step aerodynamic performance of the wind turbine was tested by using 500 W electric generator and power meter.

As it can be seen from Fig.4 the base case rotor showed highest power coefficient, Cp of 0.47 by rotor performance test, and Cp value of 0.38 wind turbine performance test at the Tip Speed Ratio (TSR) of 6.3 and the wind speed of 7 m/s. The difference of the Cp values is due to the efficiency loss during of power conversion of the generator and power electronics.

Figure 1 The 500W small HAWT

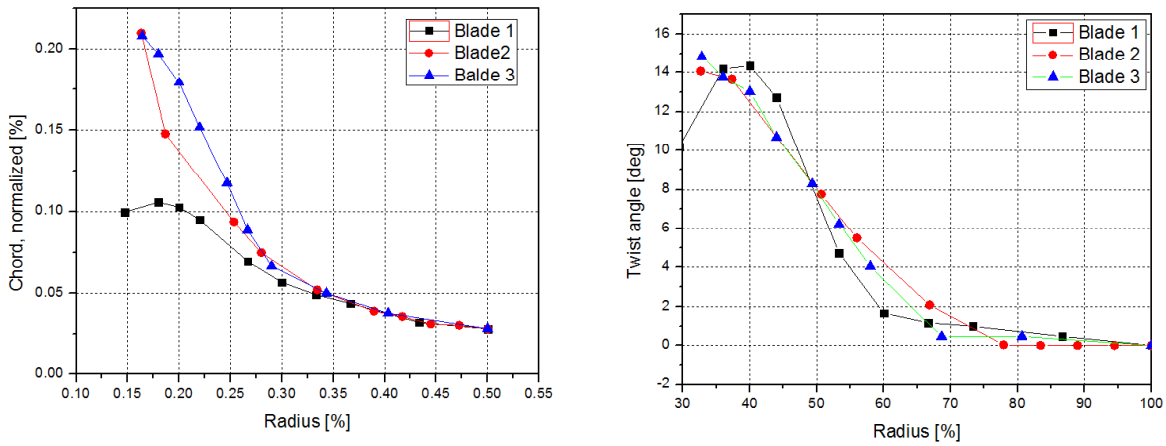

Figure 2 Chord lengths and twist angle distribution of the blade models

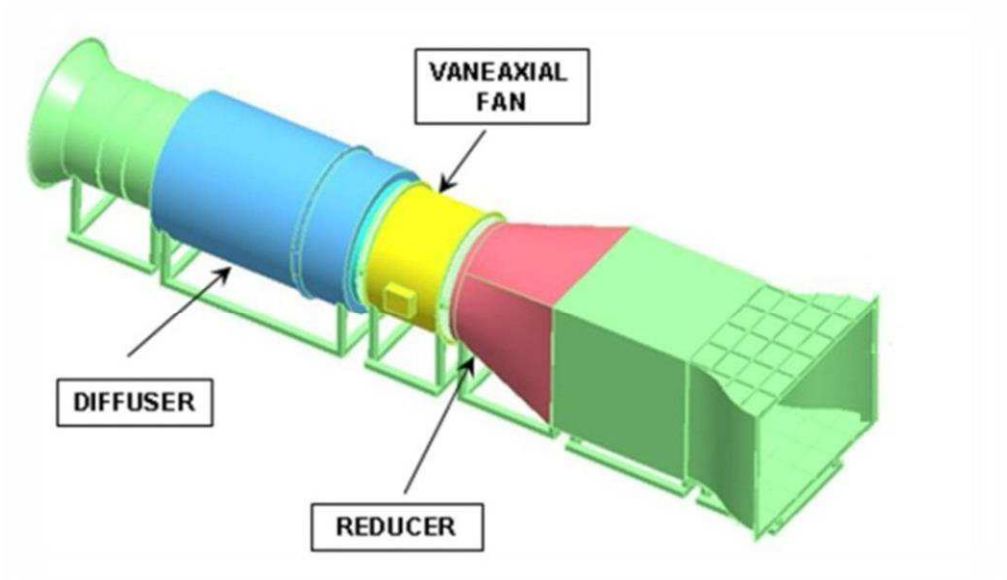

Figure 3 Open circuit low speed wind tunnel

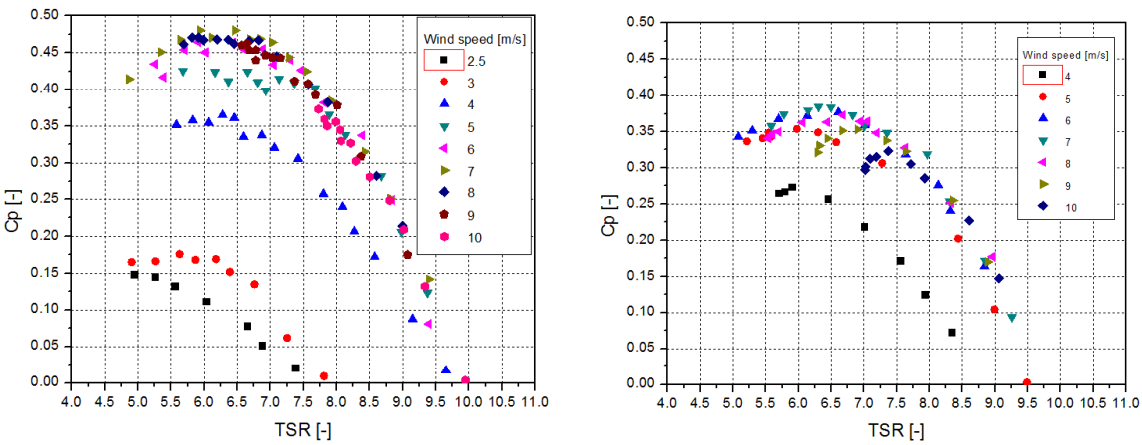

Figure 4 Wind turbine performance curves (wind tunnel test result, right: rotor performance test, left: generator performance test)

3. Aerodynamic analysis method

In the near-field flow computation neither ground nor the tower were included into the model, and uniform wind speed profile was assumed at the inlet of the domain. For the volume mesh generation the 120 degree periodicity of the rotor was exploited, and only volume around one blade was meshed. The remaining two blades were included in the computations using periodic boundary conditions.

For the meshing ANSYS ICEM CFD processor was used to build a hexahedral mesh consisting from approximately 3.6 million volume elements. The near blade region compromised H-shaped grid structure, shown in Fig.5, and it was optimized by

means of 2-D simulations to meet wall function requirement. The y+ value at the blade surface was kept less than values of two.

The SST turbulence (Menter 1994) model was used as a turbulence closure model for accurate prediction flow structure in near-field region. The three dimensional flow around rotor blades of the wind turbine had been simulated by unsteady incompressible RANS equation based on commercial solver ANSYS CFX-11.0 (Ansys 2003).

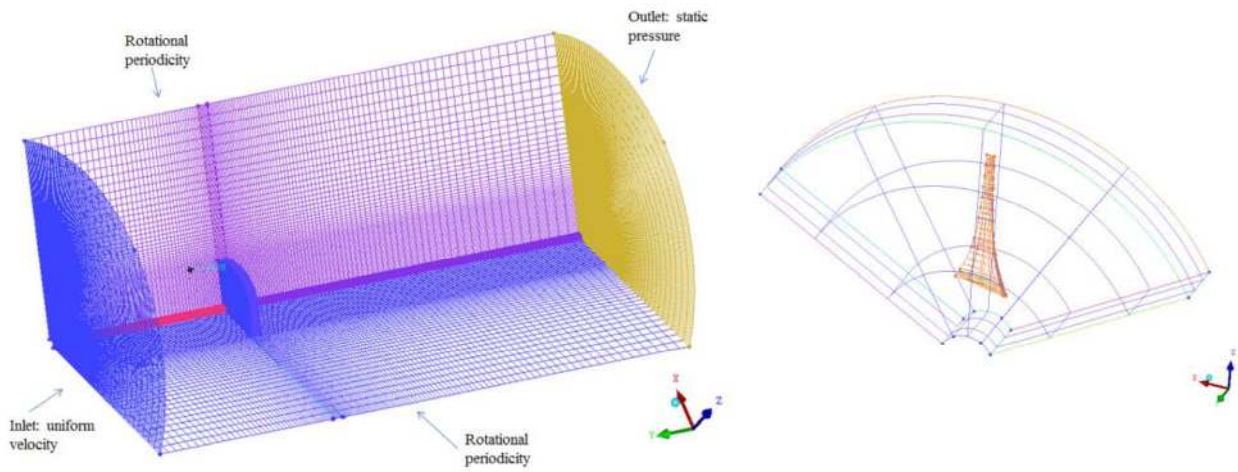

Figure 5 Computational domain and boundary conditions

The flow field in the computational domain was aerodynamically analyzed by solving three dimensional steady incompressible RANS equations with a shear stress transport (SST) transitional turbulence model on the commercial code ANSYS CFX-11.0 (Ansys 2003). The results of computations were processed by CFX-Post processor.

The total pressure and mass flow rates were set at the inlet and outlet of the computational domain, respectively. The rotating periodic boundary condition and pressure opening conditions were applied in latitudal and longitudal direction of the blade. A frozen rotor coupling method was used at the interface between rotating and stationary domains (Tennekes Limley1972).

The convergence criteria of are set to 10^{-4} of root-mean-square (RMS) residual values for all governing equations. The computations were carried out by using Intel Core I7 CPU with a clock speed of 2.94GHz.

4. Aeroacoustic analysis method

Based on steady state simulation results the unsteady RANS analysis was conducted to obtain pressure and velocity fluctuations on blade and integration surface to perform acoustic analysis. For unsteady computation time step was set to 3.8×10^{-5} seconds and coefficient loop for time scale control was set to 3. The flow simulations were obtained after at least 2,048 iterations which correspond to 4 full rotations of the rotor blades.

Di Fracescantinio (1997) published a permeable FW-H equation formulation which gives possibility to include quadrupole noise source term. The main idea of the formulation is to integrate noise source term values over fictitious surface at some distance from actual blade surface enclosing entire noise generating region. The main advantage of the Francestinio's formulation is possibility to include quadrupole source terms without expensive numerical evaluations. The permeable FH-W equation is given as:

$$\frac{1}{c_0^2}\frac{\partial^2 p\prime}{\partial t^2} - \overline{\nabla^2} p' = \frac{\partial}{\partial t}\{[\rho_0 v_n + \rho(u_n - v_n)]\delta(f)\} - \frac{\partial}{\partial x_i}\left\{\left[p'_{ij} n_j + \rho u_i(u_n - v_n)\right]\delta(f)\right\} + \frac{\overline{\partial^2}}{\partial x_i \partial x_j}\left[T_{ij} H(f)\right]. \quad (1)$$

here u_n is the fluid velocity, and v_n is the control surface velocity in the normal direction of the integral surface.

The solution of the permeable FH-W equation is given as

$$4\pi p'(x,t) = \int_{f=0}\left[\frac{\rho_0(\dot{U}n + U\dot{n}}{r(1-M_r)^2}\right]_{ret} dS + \int_{f=0}\left[\frac{\rho_0 U_n(r\dot{M}_i r_i + c_0 M_r - c_0 M^2)}{r^2(1-M_r)^3}\right]_{ret} dS$$
$$+\frac{1}{c_0}\int_{f=0}\left[\frac{\dot{L}r}{r(1-M_r)^2}\right]_{ret} dS + \int_{f=0}\left[\frac{Lr - L_i M_i}{r^2(1-M_r)^2}\right]_{ret} dS + \frac{1}{c_0}\int_{f=0}\left[\frac{Lr(r\dot{M}_i r_i + c_0 M_r - c_0 M^2}{r^2(1-M_r)^3}\right]_{ret} dS \quad (2)$$

where:

$$U_i = \left(1 - \frac{\rho}{\rho_0}\right) v_i + \frac{\rho u_i}{\rho_0} \text{ and } L_i = p_{ij} n_j + \rho u_i(u_n - v_n). \quad (3)$$

5. Validation of numerical results

To validate numerical simulation of flow field and in-house developed noise prediction code a two-step process were applied. At the first step, the numerically predicted aerodynamic performance characteristic of the rotor was compared with the wind tunnel experimental data. As shown in the Fig. 6, the numerically predicted performance curve showed good agreement with data obtained in wind tunnel experimental test data.

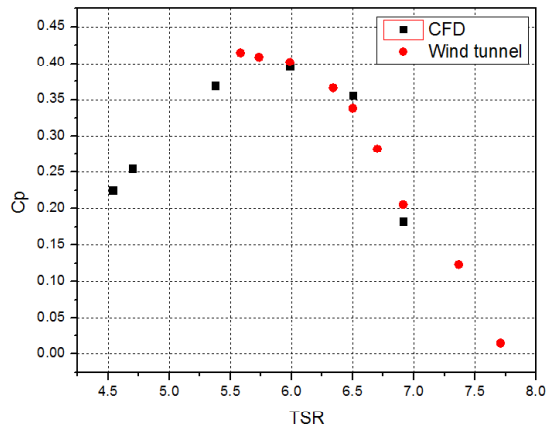

Figure 6 Power performance of blade set two at 5 m/s wind speed

As next step, the noise signature of axial-fan was predicted using in-house developed code. The axial-flow fan specifications and blade section profiles used for the validation is shown in Table 1 and Fig. 7 respectively (Kim 2011). The noise signature of the axial-flow fan was experimentally tested in Fluid machinery test center according to the AMCA standards (AMCA 2005). The numerically predicted and experimentally tested sound power level of axial-flow fan is shown in Fig. 8.

Table 1 Design specifications of the axial flow fan

Design volume flow rate, m^3/min	60
Rotational speed, rpm	1170
Pressure rise, Pa	100
Tip diameter, mm	510
Hub-to-tip ratio	0.294
Tip clearance, mm	2
Number of blades	10

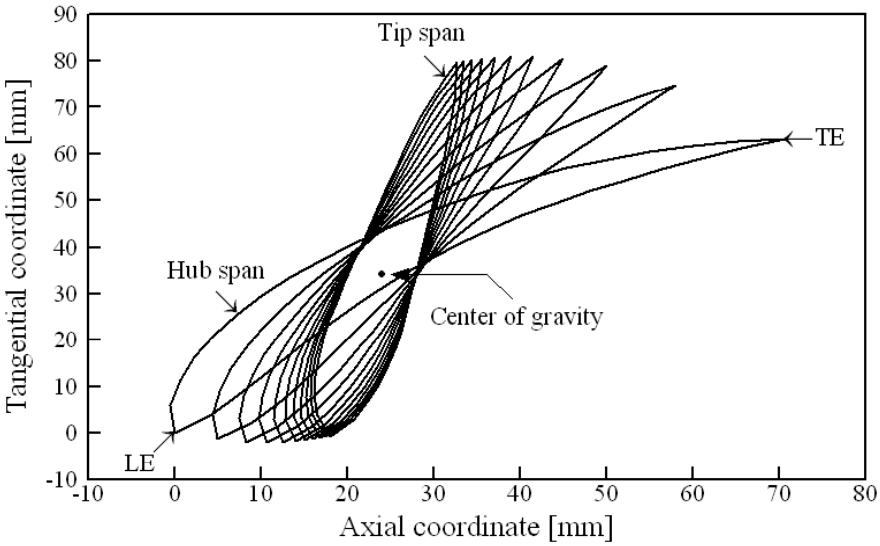

Figure 7 Sections of blade profiles from hub to tip (Kim 2011)

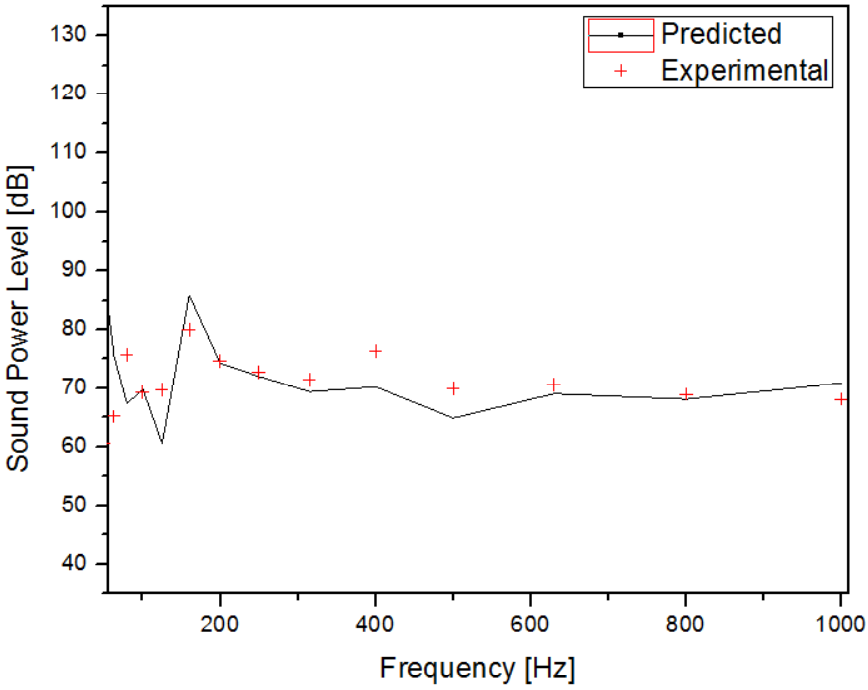

Figure 8 One third octave band sound power spectrum

6. Results and discussions

The power performance of the rotor blades are analyzed and compared by non-dimensional parameter for power coefficient. For the analysis three sets of blades, shown in Fig. 9, are used. In the Fig. 10 is shown the CFD predicted Cp of the three sets of the blades at different TSR. The simulation results suggest that the all blades reach their maximum efficiency at TSR of 6. The highest efficiency is expected for Blade 2 with value of Cp 0.39 and the lowest efficiency for the Blade 1 with value of Cp 0.34. The geometries of the blades suggest that they have similar dimensions at the blade tip region and very different dimension at the blade root section. In the Fig. 4.6 is shown the pressure coefficient distribution along chord length at 10, 40 and 90 percent of the rotor radius. At 10% of the rotor radius the Blade 3 has 38% longer, and the Blade 1 has 42% shorter chord length than the Blade 2.

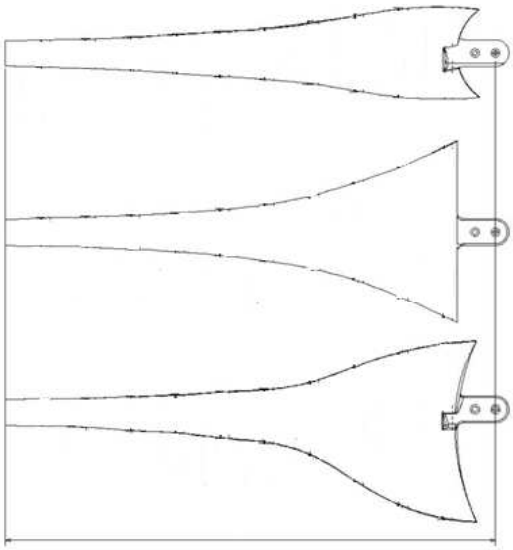

Figure 9 Geometry of three blade models (from top to bottom: Blade 1, Blade 2 and Blade 3)

As it can be seen from Fig. 11 a) the Blade 1 has highest negative pressure distribution on suction side which leads to higher lift force generation per unit chord length. The Blade model 3 has the lowest pressure distribution on the blade surface which corresponds to lowest lift force generation per unit chord length. A similar condition is also observed at 40% of rotor radius. The Blade model 1 has the highest pressure distribution but 14% shorter chord length than Blade model 2. The Blade 3 also is 5% shorter chord length than Blade model 2 and also gives the smallest pressure distribution along blade surface. In the overall, although the Blade model 1 has the highest pressure distribution at all positions, which corresponds to higher lift force per unit length of chord, but due to large geometrical difference it end up lowest lift force generation on entire blade. As results the Blade model 2 ends up with higher overall rotor power efficiency.

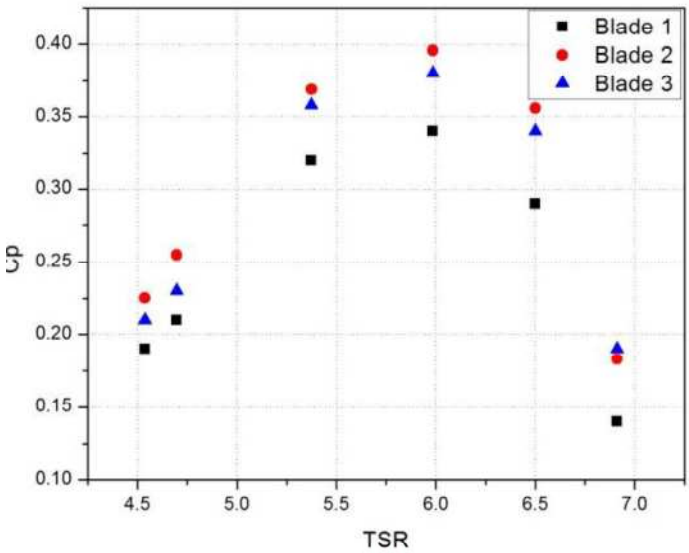

Figure 10 Power performances of the three blade models

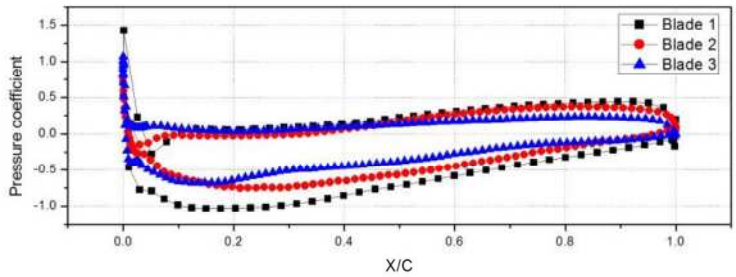

a) At 10 % of blade span

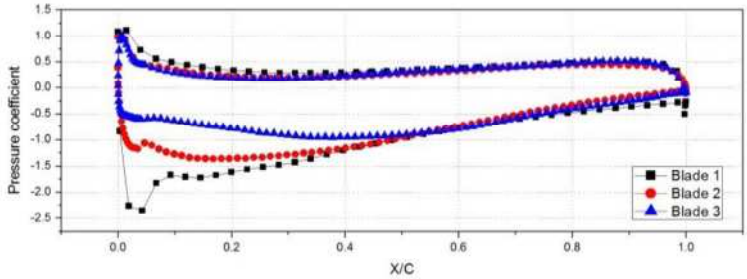

b) At 40% of blade span

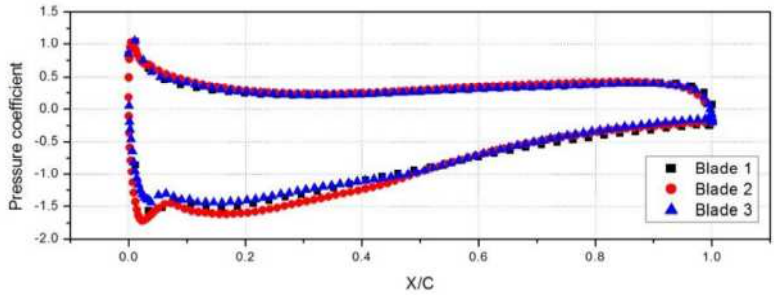

c) At 90% of blade span

Figure 11 Pressure coefficient distribution of the blade surface at wind speed of 5 m/s

The acoustic characteristics of the blades are evaluated in terms of sound pressure spectrum and overall sound pressure level. The analysis for the case of uniform incoming wind speed of 5m/s with 15% turbulent intensity, observer location of 12.75 m down wind at 12 m below the hub of wind turbine is performed. The observer location is determined according to IEC 61400-11 standard as shown in Fig. 12 (IEC 61400-11 2006). For the validation the numerical data of power performance and acoustic simulation results are compared with experimental data by wind tunnel test and acoustic measurement data in open air environment.

The resulted non-weighted and A weighted sound pressure level spectrum is shown in Fig.12 and Fig.13 respectively. The Overall Sound Pressure Level (OSPL) at observer location is estimated as 46.36 dB for Blade model 1, 46.55 dB for Blade model 2 and 51.46 dB for Blade model 3 respectively. Close examination of sound pressure spectrum reveals that Blade model 1 showed the lowest for all frequencies

and at low frequency range Blade model 2 has highest but for higher frequencies Blade model 3 showed highest sound pressure levels.

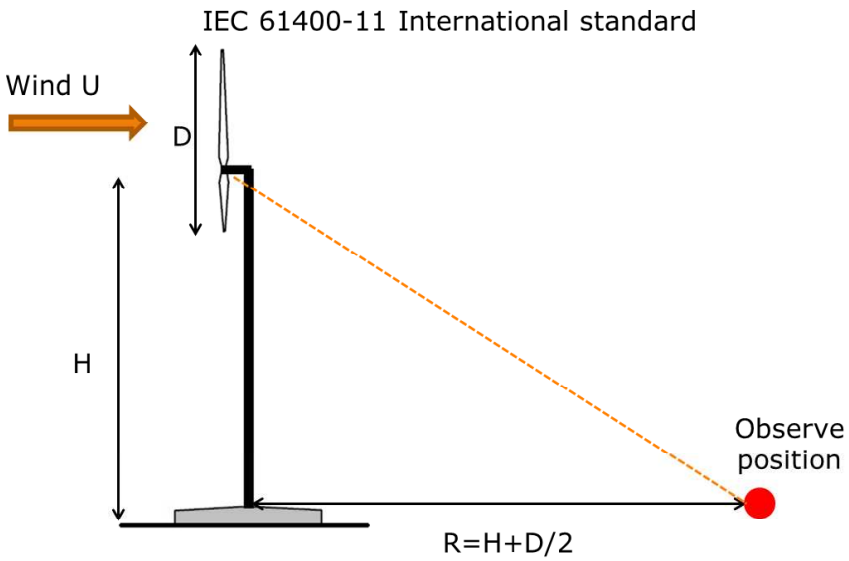

Figure 12 The microphone position

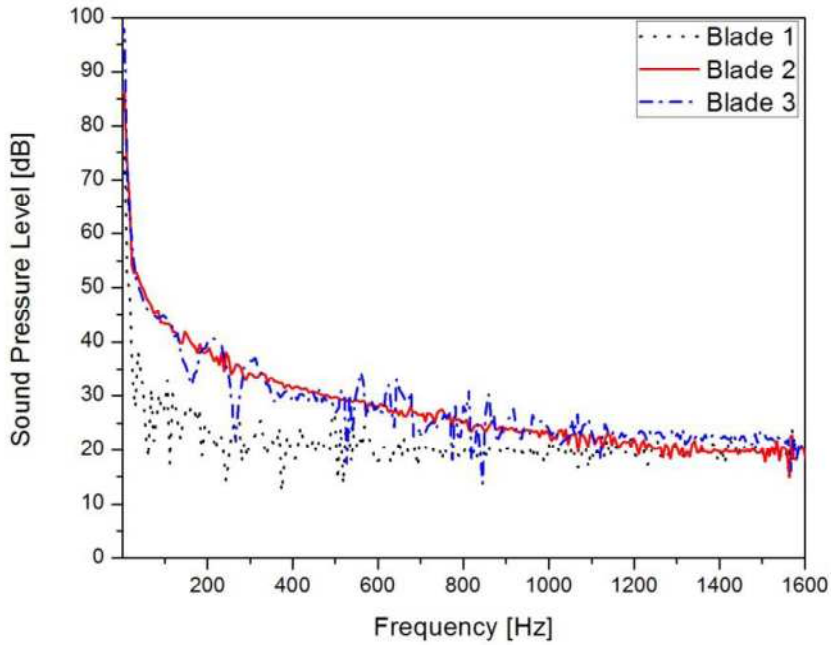

Figure 12 Sound pressure level for analyzed blade sets

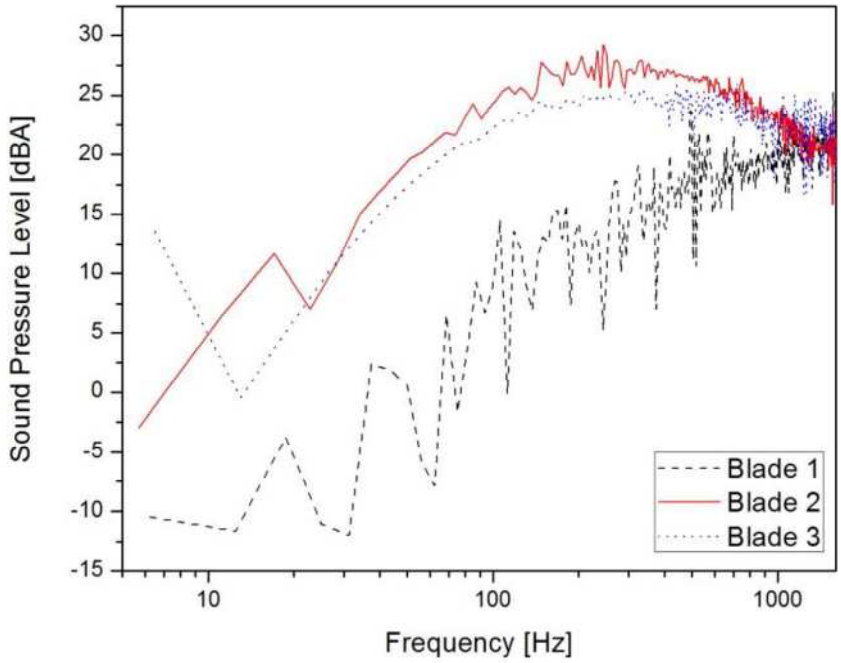

Figure 13 A-weighted sound pressure level for analyzed blade sets

7. Conclusions

The numerical analysis of aerodynamic performance and acoustic characteristics of three sets of blades with different chord length and twist angle distributions were analyzed by use of commercial steady and unsteady Reynolds-averaged Navier-Stokes solver and in-house acoustic code based on permeable surface formulation FW-H equations.

The power performance evaluation revealed that Blade model 2 model has the best power performance with power coefficient value of 0.39 and lowest performance is observed for the Blade model 1 model with power coefficient of 0.34. The Blade model 2 and 3 show similar power performance characteristics.

The overall sound pressures at the predetermined observer location are estimated as 46.36 dB, 46.55 dB, and 51.46 dB for blade models 1, 2, 3, respectively.

The current study analyzed an aeroacoustic performance analysis method for small wind turbine rotor blades. The method applied for small wind turbine rotor blades showed good agreement with experimental data.

ACKNOWLEDGEMENT

This work is the outcome of a Manpower Development Program for Marine Energy by the Ministry of Land, Transport and Maritime Affairs (MLTM).

References

Casper J, Farassat, (2002), *A New Boundary Integral Formulation for the Prediction of Sound Radiation,* AIAA paper No.2002-0802, 40thAerospcae Science Meeting and Exhibit, Reno, NV, USA

Ianniello S (2007) *New Perspectives in the Use of the Ffowcs Williams-Hawking's Equation for Aeroacoustic Analysis of Rotating Blades,* Journal of Fluid Mechanics, 570, 79-127

Lyrintzis AS (1994) *Review: The Use of Kirchhoff Method in Aeroacoustics,* ASME Journal of Fluids Engineering, 116, 665-676

Lyrintzis AS (2003) *Surface Integral Methods in Computational Aeroacoustics – From the (CFD) Near-field to the (Acoustic) Far-field,* International Journal of Aeroacoustics, 2(2), 95-128

Bogey C, Bailly C and Juve D (2002) *Computation of Flow Noise Using Source Terms in Linearized Euler's Equations*, AIAA Journal, 40(2), 235-243

Tadamasa A, Zangeneh M (2011) *Numerical Prediction of Wind Turbine Noise,* Renewable Energy, *36, 1902-1912*

Menter FR (1994) *Two-Equation Eddy-Viscosity Turbulence Models for Engineering Applications,* AIAA Journal, 32(8), 1598-1602

Ansys CFX Solver Theory, Ansys Inc.,

Tennekes H, Limley JL, *A First Course in Turbulence*, The MIT Press, Cambridge, 1972

DiFracesscantinio P (1997) *A New Boundary Integration Formulation for the Prediction of Sound Radiation,* Journal of Sound and Vibration, 202(4), 491-509

Kim JH, Kim JW, and Kim KY (2011) *Axial-Flow Ventilation Fan Design Through Multi-Objective Optimization to Enhance Aerodynamic Performance,* ASME Journal of Fluids Engineering, 133(10), 101101

AMCA Standard 300-05 Reverberant Room Method for Sound Testing of Fans, 2005

Wind turbine generator systems-Part 11: Acoustic noise measurement technique. IEC 61400-11 International Standard IEC 2006